Journal of Materials Processing Tech. 261 (2018) 184–192

Contents lists available at ScienceDirect

Journal of Materials Processing Tech.

journal homepage: www.elsevier.com/locate/jmatprotec

Tensile behavior of fusion-brazed aluminum alloy coach-peel joints fabricated by a dual-beam laser

Guang Yang[a], Jie Sheng[a], Wei Tong[a], Blair E. Carlson[b], Hui-Ping Wang[b], Radovan Kovacevic[a,*]

[a] Department of Mechanical Engineering, Southern Methodist University, Dallas, TX, 75206, United States
[b] General Motors, R&D Laboratories, Warren, MI, 48092, United States

ARTICLE INFO

Keywords:
Coach-peel joint
Image-based finite element analysis
Strain hardening model
Fusion-brazed

ABSTRACT

As the stress-strain data of the fusion-brazed filler material AA4047 could not be easily or directly measured, an isotropic strain-hardening model of the fusion zone material AA4047 was estimated by an inverse method to quantify the tensile behavior of AA6111-T4 coach-peel joints. The Hill's 1948 quadratic anisotropic yield stress function for the base sheet metal AA6111-T4 was first determined by conducting uniaxial tensile tests on the sheet metal in the rolling, diagonal, and transverse directions. Based on the yield stress function and isotropic strain hardening behavior determined for the base sheet metal, the linear-exponential strain hardening model was used to identify the fusion zone material AA4047 by an iterative correction and image-based finite element analysis of the welded joint. Modeling of joints with and without flawed brazing interface showed that the load-carrying capacity of coach-peel joints was insensitive to the existence of the brazing zone metal AA4047. When the fusion zone model was also applied to the brazing zone, the predicted and measured force-displacement curves of the coach-peel joint matched well. The failure stress of the coach-peel joint was identified as the von Mises fracture stress of 100 MPa at the brazing interface.

1. Introduction

Developments of the laser joining technology allow the design of automotive components to be simplified and bring a significant improvement in the exterior appearance of a car. For example, the roof and side member panels can be directly attached to channel the rainwater away without using the unsightly roof drip molding. Aluminum alloy 6111-T4 coach-peel panels laser-joined with AA4047(AlSi12) filler wire have been widely applied in automotive bodies. Yang et al. (2017a) compared a side-by-side dual beam (cross-beam) laser, an in-line dual beam laser, and a single beam laser with the same processing parameters for joining of coach-peel panels. They found that the relatively lower energy density of cross-beam laser induced a weaker convection within the molten pool and a faster solidification rate at the weld surface. Consequently, it was easy to generate the fusion-brazed joints with a good weld surface quality and a small heat affected zone by a cross-beam laser; the temperature gradient distributions also contribute to the long dendrites in the fusion zone but only Si-particles in the brazing zone (Fig. 1). The mechanical performance of a joint is determined by material properties in different zones as well as structural features, such as the joint geometry and the internal defects. The fusion-based joint can be rendered as an assembly that is composed of the base metal and two sections of the weld bead. The heat affected zone (HAZ) can be neglected as its thickness was ~ 100 μm, or 1/12 of the panel thickness (Fig. 1a). A complete structural analysis of coach-peel joints is essential to evaluate the strength of the aluminum alloy structure, and instructive for improvement of the manufacturing process. In order to model the mechanical response of a coach-peel joint, the strain-stress data of each material are required.

A mini-tensile test of weld materials is the most popular test to directly characterize their mechanical properties. Tong et al. (2005) investigated the plastic deformation of miniature tensile bars cut from the resistance-spot-weld up to the rupture failure. Ma et al. (2014) machined the mini-tensile coupons from the weld bead, the heat affected zone, and the substrate of the lap joints, and examined their tensile behaviors. Unfortunately, it was too difficult and impractical to machine flat coupons from the weld section of a coach-peel joint as shown in Fig. 1b. Even if the mini-tensile coupons of small size were machined from the weld bead, the relatively brittle nature of AA4047 could easily induce premature fracture at the shoulder section of the tensile coupon. Due to these two reasons, it is not suitable to determine the tensile stress-strain data of the fusion-brazed material AA4047 even with strain measurements by the digital image correlation as Sierra et al. (2008) advocated. A plausible alternative solution to acquire a stress-strain

* Corresponding author.
E-mail address: kovacevi@smu.edu (R. Kovacevic).

https://doi.org/10.1016/j.jmatprotec.2018.06.016
Received 6 September 2017; Received in revised form 12 June 2018; Accepted 13 June 2018

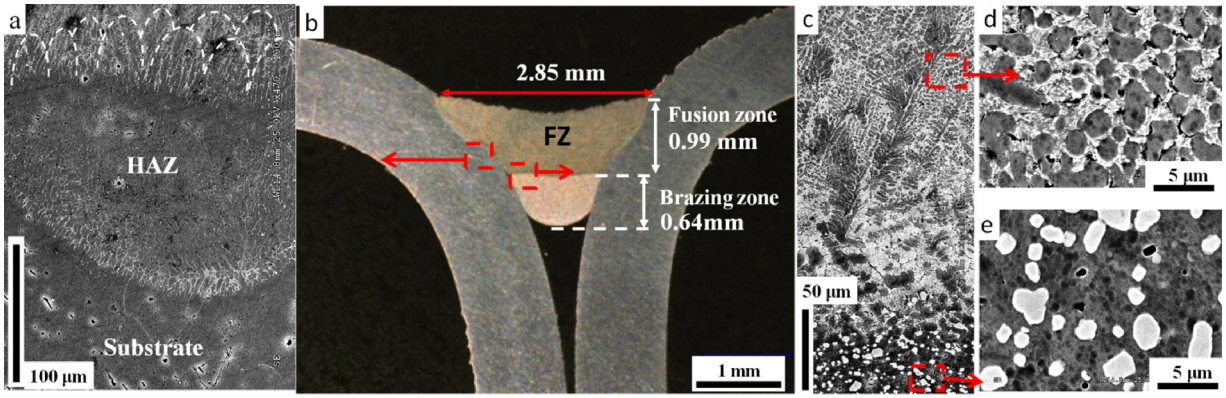

Fig. 1. Microstructures of the cross-beam joint prepared at a laser power of 4 kW and characterized by Yang et al. (2017a). (a) Heat affected zone, (b) cross-section of the joint, (c) eutectic mushy zone, (d) eutectics and dendrites in the fusion zone, (e) Si particles in the brazing zone.

relationship of the weld material is an inverse method based on numerical FE simulations. An assumed analytical model of isotropic strain hardening of AA4047 may be iteratively calibrated and corrected in a virtual tensile test via the finite element analysis (FEA) by minimizing the differential between the measured and predicted stress-strain relationship of the joint. This method is typically used to study the pre-necking and post-necking strain hardening behavior of the same material under uniaxial tension and has so far proven to be very successful by Wang (2015) and Wang and Tong (2015).

Many anisotropic yield functions and stress-strain relationships for isotropic hardening can be applied to describe the plastic deformation up until fracture initiation. For example, Tong (2005) mathematically formulated an anisotropic plasticity model by using the orthogonal series expansion in both the principal stress space and the loading orientation space. This model could describe the directional dependence of flow stress, plastic strain ratio, evolution of isotropic hardening, and macroscopic plastic spin ratio for a large variety of textured polycrystalline sheet metals. Panda et al. (2008) adjusted the K and n values in the power-law equation of $\sigma = K\varepsilon^n$ for the heat affected zone after laser scanning of DP980 steel. Tao et al. (2009) proposed an iterative correction procedure using FEA to accurately determine the effective true stress- true strain curves of sheet metals. The procedure went beyond the testing for diffuse necking strain levels and included testing with various strain hardening behaviors and tensile coupon geometries. Yang and Tong (2009) implemented several plasticity models to evaluate the base metal, heat-affected zone, and weld metals of a dual-phase steel DP600. They summarized an effective approach to construct an advanced strain hardening model based on several simple isotropic strain-hardening models, such as linear hardening (L), Voce exponential hardening (E), and Swift power-law hardening (P), as provided in Eq. (1).

$$\begin{aligned}
\sigma(\varepsilon^p) &= \sigma_u\,(1 + \varepsilon_e^p - \varepsilon_u) && \text{(L model, 1–1)}\\
\sigma(\varepsilon^p) &= \sigma_u\left(1 + \varepsilon_0\left(1 - e^{\frac{\varepsilon_u - \varepsilon_e^p}{\varepsilon_0}}\right)\right) && \text{(E model, 1–2)}\\
\sigma(\varepsilon^p) &= \sigma_u\left(\frac{\varepsilon_e^p + \varepsilon_0}{\varepsilon_u + \varepsilon_0}\right)^{\varepsilon_u + \varepsilon_0} && \text{(P model, 1–3)}
\end{aligned} \tag{1}$$

where ε^p, ε_0, σ_u, ε_u are an effective true plastic strain, a positively-valued material model parameter, and the true stress-true strain data at the onset of diffuse necking. Wang and Tong (2015) suggested a local correction factor method for identifying the post-necking strain hardening behavior of metals. This method could extend the classical Bridgman approach to thin sheet metals with non-symmetric, irregular necking morphologies and with a general non-quadratic anisotropic flow function.

The models and correction procedures proposed by Tao et al. (2009), Yang and Tong (2009), and Wang and Tong (2015) suggested that an inverse method via the image-based finite element modeling could be applied to accurately determine the isotropic strain hardening behavior of the weld material AA4047. The linear-exponential law (LE) has less material parameters to calibrate than the exponential-power (EP) and the linear-exponential-power law (LEP). Therefore, the LE model of the base metal AA6111-T4 was first obtained from uniaxial tensile test data and used as the initially estimated strain-hardening model of AA4047 in this study. By applying stress and strain on continuum material elements, the plasticity model of the fusion-brazed AA4047 was iteratively corrected until the predicted load-displacement curve of the coach-peel joint matched with the measured mechanical response. The derived LE model of AA4047 could be easily used to reconstruct strain-stress data of this material for a virtual uniaxial tensile testing in the future.

In the real manufacturing, many factors, such as the surface condition of the panel described by Yang et al. (2017c) and the laser-wire-gas nozzle position discussed by Yang et al. (2017b), could change the molten pool dynamics and the wettability of the filler wire, further generating the imperfections at the brazing interface close to the bottom of the weld bead. The flawed brazing interface in the coach-peel joint was modeled as a gap between the brazing zone and the substrate. Through the exploration of the load-carrying capability of the weld, further quality control decisions might be made to define the Class-A laser weld in the automotive industry.

2. Experiments

Tables 1 and 2 show the material and welding parameters. AA6111-T4 aluminum alloy panels with a thickness of 1.2 mm were joined with the addition of AA4047 filler wire by the cross-beam fiber laser at a laser power of 4 kW, a welding speed of 60 mm/s, and a wire feed rate of 70 mm/s. Detailed parameter optimization and microstructure evolution of the cross-beam laser weld could be found in Ref. (Yang et al. (2017a) and Yang et al. (2017b)). The mechanical analysis of the coach-peel joint follows four steps as illustrated in Fig. 2:

(1) Characterize the anisotropic yield function of the base metal AA6111-T4 (Material 1);
(2) Estimate the isotropic strain-hardening model of the fusion zone metal AA4047 (Material 2);

Table 1
Chemical composition (wt. %).

Alloy	Si	Fe	Cu	Mn	Mg	Ti	Al
AA4047	12.55	0.43	0.05	0.18	0.05	0.1	rest
AA6111-T4	0.63	0.5	1.15	0.57	1.43	0.48	rest